Dry reforming of methane in a rotating gliding arc plasma: Improving efficiency and syngas cost by quenching product gas

Hyoungjoon Kwon[a], Taewoo Kim[b], and Soonho Song[a,*]

[a] Department of Mechanical Engineering, Yonsei University, 50 Yonsei-ro, Seodaemun-gu, Seoul, 03722, South Korea
(E-mail: kwon.h.jay@yonsei.ac.kr, soonhosong@yonsei.ac.kr)
[b] Department of Mechanical Science and Engineering, University of Illinois at Urbana-Champaign, Urbana, Illinois 61801, USA
(E-mail: tk21@illinois.edu)

*** Corresponding author**
Address: Department of Mechanical Engineering, Yonsei University, 50 Yonsei-ro, Seodaemun-gu, Seoul, 03722, South Korea
Telephone: +81-2-2123-2811
E-mail: soonhosong@yonsei.ac.kr

Abstract

Rotating gliding arc (GA) plasma has attracted increasing interest in dry reforming of methane (DRM) for CO_2 utilization. Most DRM studies using GA plasma are conducted to improve energy efficiency by increasing the conversion of reactants. This study aimed to improve energy efficiency by increasing the selectivity of products, particularly that of H_2. To increase the selectivity of H_2, a quenching device (i.e., a quenching rod (QR)) was developed to protect H_2 from being consumed by suppressing the reverse water–gas shift (RWGS) reaction that is dominant in CO_2 and H_2 consumption in DRM processes. When the QR was applied, the conversion of CH_4 and CO_2 was reduced, while the selectivity and yield of H_2 and H_2O changed significantly, i.e., the yield of H_2 increased, and the yield of H_2O decreased. Owing to the increased yield of H_2, the energy efficiency and syngas cost were improved. At an SEI of 4.2 kJ/L with a CH_4/CO_2 ratio of 5/7, the conversion of CH_4 and CO_2 was 51.1% and 40.2%, respectively; the highest energy efficiency was 55.3% with syngas costs of 10.9 kJ/L. Moreover, compared with the results of other DRM studies, syngas with the highest H_2/CO ratios of 0.95 and 1.26 at CH_4/CO_2 ratios of 5/7 and 1 was produced with the reactor applied in this study, respectively. In conclusion, optimizing the quenching process will probably further improve the DRM performance. Moreover, the quenching method will be applied to dry reforming processes for syngas with high H_2/CO ratios.

Keywords: Warm plasma**,** Dry reforming of methane, Reverse water–gas shift reaction, Quenching, Syngas production

1. Introduction

CO_2 utilization technology, which converts CO_2 into value-added chemicals, has attracted significant interest because it may mitigate global warming issues [1]. In dry reforming of methane (DRM), CO_2 and CH_4 are converted into syngas (i.e., an H_2/CO mixture), as shown in reaction (R1). This reaction is environmentally and economically desirable as it uses the two main greenhouse gases CO_2 and CH_4 simultaneously and produces syngas that can be converted into higher-value chemicals through a Fischer–Tropsch (FT) process after further adjustment of the H_2/CO ratio [2-4].

$$CH_4+CO_2 \rightarrow 2CO+2H_2 \quad \Delta H^\circ = 247\ \text{kJ/mol} \tag{R1}$$

The high reaction enthalpy (ΔH°) of (R1), which arises from the inert and stable characteristics of both reactants (i.e., CH_4 and CO_2), implies that this reaction is strongly endothermic. Hence, DRM is unfavorable under ambient conditions [5-7]. The conventional DRM process has been carried out thermo-catalytically to activate the reaction easily; however, the high-temperature condition (approximately $800^\circ C$) is still required. In addition, owing to catalyst deactivation by carbon deposition, conventional catalytic DRM has not been applied in the industry [6, 7].

Non-thermal plasma can be a promising alternative for overcoming the deficiencies of conventional catalytic DRM. Non-thermal plasma can be obtained through the following processes. When electrical energy is applied to a reactor and selectively transferred to heat electrons, these accelerated electrons collide with gas molecules to create highly reactive particles, such as excited species, radicals, ions, and photons [8]. During the collisions of electrons and gas molecules, a tiny portion of electron energy is lost because electrons are much lighter than gas molecules, thereby leading to a significant difference between the temperature of electrons (order of a few eV) and that of the gas (room temperature to a few thousand Kelvin) [8, 9]. This thermodynamic non-equilibrium of the non-thermal plasma allows thermodynamically unfavorable reactions to occur under mild conditions [9-11].

Among the various types of non-thermal plasmas (such as dielectric barrier discharge, microwave discharge (MW), nanosecond-pulsed discharge, and gliding arc (GA) discharge plasmas), GA and MW plasmas are considered warm plasmas by the researchers of [9, 12-14] owing to their inherent higher gas temperatures. Depending on the plasma type, the operating range of the reduced electric field is different, thereby affecting the electron energy distribution [9]. The warm plasma operates in a relatively low reduced electric field in which a significant fraction of the electron energy is transferred to the vibrational excitation of molecules, which is known to play a vital role in activating and reacting stable molecules such as CH_4 and CO_2 [8]. In addition, as the gas is heated through vibrational–translational (VT) relaxation, the warm plasma has a higher gas temperature (1000–3000 K) than other non-thermal (cold) plasmas (near room temperature) [12, 14, 15]. In this highly thermal environment, successive thermal conversions can occur after the vibrational excitation-induced conversion (i.e., plasma conversion). Thus, in the warm plasma, endothermic reactions (such as DRM and CO_2 decomposition) can be activated in an energy-efficient way.

Indeed, owing to the higher gas temperatures, GA plasma shows the most promising results for DRM in terms of energy efficiency and energy cost among the mentioned non-thermal plasmas [12, 14, 16-23]. Until recently, DRM studies with GA plasma have been conducted to improve the energy efficiency by reinforcing the higher gas temperature characteristics of GA plasma; the energy efficiency of DRM has been increased through increased thermal conversion of CH_4 and CO_2, which were induced by increasing the gas temperatures by varying the operating parameters. Dinh et al. [21] analyzed the heat transfer characteristics with different configurations of the reactor through experiments and 3D modeling; according to their results, when a nozzle-type reactor was applied rather than a diverging-type reactor, heat loss to the reactor wall was reduced, and the downstream gas temperature was higher. Consequently, the energy efficiency and conversion were improved in the nozzle-type reactor (energy efficiency of 53% at the conversion of CH_4 and CO_2 of 74 % and 49 %, respectively). In another study, the effect of adding N_2 as an additive on the DRM performance was investigated [22]. The experiments and computational models confirmed that most N_2 energy obtained from collisions with electrons was released through VT relaxation since most N_2 remains unconverted. As a result, the gas temperature increases significantly from 3200 K in the absence of N_2 to 4400 K when 80% N_2 is added, thereby increasing the thermal conversion of CH_4 and CO_2. At a 20% N_2 fraction in which the dilution effect of N_2 was minimized, the maximum energy efficiency was 58%, and the minimum energy cost was 8.7 kJ/L [22].

In general, the energy efficiency of DRM was improved through an increase in temperature and the thermal conversion of downstream gas, as mentioned in the above studies. However, higher energy efficiency can also be achieved by increasing the selectivity of products. For instance, if more desirable products (such as H_2 and CO) and fewer undesirable by-products (i.e., H_2O and carbon) are produced from similar amounts of converted CH_4 and CO_2 (via DRM), the energy efficiency and energy cost can be improved. The reports of the state-of-the-art DRM studies in which the authors used GA plasma presented a high selectivity of CO in the range of 80% to 90% for C-based selectivity, with C_xH_y and carbon accounting for the remaining percentage. On the contrary, for H-based selectivity, the authors reported a relatively low H_2 selectivity of 60% to 80% [12, 17, 18, 21, 22, 24, 25], with the other 20% to 30% H-based selectivity being occupied by H_2O selectivity [22, 26]. In this regard, they revealed that the relatively low selectivity of H_2 for DRM in GA plasma is ascribed to the reverse water–gas shift (RWGS) reaction (R2), which is thermodynamically feasible at high temperatures, since DRM is accompanied by the RWGS reaction in the high temperature downstream of GA plasma [27-30].

$$CO_2+H_2 \rightarrow CO+H_2O \quad \Delta H^\circ = 41 \text{ kJ/mol} \tag{R2}$$

Promoting the RWGS reaction by increasing the temperature of downstream gas can result in a high conversion of CO_2 for DRM but also a low selectivity and yield of H_2; this means that an excessive adjustment process is required to increase the H_2/CO ratio before the FT process, which increases the energy cost for syngas production. Furthermore, the high-temperature environment downstream often causes significant heat loss. Conversely, if the RWGS reaction is restrained by quenching the hot downstream gas, the conversion of CO_2 is inevitably reduced, while the selectivity of H_2 is higher and heat losses to the reactor wall and undesirable reactions are mitigated.

Quenching high-temperature gases can stop chemical reactions from proceeding; thus, by quenching the products produced in the high-temperature downstream, the target products can be saved from being consumed. Indeed, in studies of the plasma-based CO_2 decomposition [31-36], including the present authors' work [37], energy efficiency was improved by quenching hot product gas and preventing undesirable reactions (such as the recombination of CO into CO_2). However, the quenching effect on DRM has yet to be investigated; at this point, a question arises on whether quenching can suppress the RWGS reaction to increase the selectivity of H_2 and, consequently, improve the energy efficiency and energy cost. In this work, a rotating gliding arc (RGA) plasma reactor was adopted as a plasma source for DRM. The RGA plasma reactor, which is a modified conventional two-dimensional GA plasma reactor, performs uniform gas treatment owing to the three-dimensional rotating motion of the feed gas entering through tangential inlets; this reactor has been employed for various reforming processes [12-14, 16-19, 21, 25, 38-41]. In addition, to suppress thermal reactions, particularly RWGS reaction, a water-cooled quenching device was developed and applied downstream of the reactor. Before the experimental investigation of the DRM performance, thermodynamic equilibrium analysis was conducted to have insight into the influence of RWGS reaction on DRM. Subsequently, the effect of quenching on the DRM performance was experimentally evaluated with different CH_4/CO_2 ratios and input powers. The obtained DRM performance was compared with those reported in previously published works. The results of this study demonstrate the feasibility of quenching as a plasma parameter to improve the DRM efficiency.

2. Experiments

2.1. RGA reactor configuration and cooling system

As shown in Fig. 1, the used RGA plasma system consists of three parts: the RGA reactor, electrical circuit, and gas analysis system. The RGA reactor comprises an inner electrode, an external electrode with four tangential inlets, a nozzle outlet, and a quenching rod (QR). Ceramic rings are inserted between the two electrodes and between the external electrode and QR for electrical insulation. The inner electrode is made of copper and has a conical shape with a full diameter of 32 mm. The external electrode is made of stainless steel, and the inner diameter of the body is 36.2 mm. Therefore, the shortest gap between the inner and external electrodes in which the arc ignition occurs is approximately 2.1 mm. In addition, four tangential inlets (diameters of 2 mm) were drilled into the external electrode such that the feed gas is injected in a swirling motion. By using the nozzle and tubular outlet (diameter of 16 mm), the gas flow formed a torch-like flow and a recirculation zone near the arc, which greatly extended the gas residence time in the arc plasma [17, 42].

Moreover, cooling systems were applied to operate the reactor safely and quench the product gas rapidly. Once the arc discharge ignites in the shortest gap, it is pushed downstream of the reactor by the rotating flow of the feed gas entering through the tangential inlets and elongating along the outer electrode wall and inner electrode. Heat energy from the arc was focused on the inner electrode tip. To prevent melting, the inner electrode was continuously cooled with cold water (approximately 20 °C). By contrast, the external electrode was not water-cooled since the heat was dissipated to a relatively large area. Another water cooling system was used for the QR, which is a scaled-up version of the QR developed in [37]. This quenching device was developed to lower quickly the temperature of the product gas undergoing thermal conversion as it was continuously cooled with cold water (approximately 7 °C) and implemented downstream of the reactor, 20 mm from the tubular outlet. Quenching the hot product gas with the QR can be expressed as the convective heat transfer as follows:

$$\dot{Q} = hA(T_g - T_s) \tag{E1}$$

where $\dot{Q}$ is the heat transfer rate, h is the heat transfer coefficient, A is the surface area for heat transfer, and T_g and T_s are the gas and surface temperatures, respectively. When the QR is submerged in product gas from the tubular outlet, a stagnation point is formed at the QR tip, which reduces the local velocity of the gas to zero, thereby resulting in a higher heat transfer coefficient [43]. In addition, using the QR increases the surface area for heat dissipation. Lastly, since the QR is cooled with cold water much cooler than the product gas, the temperature difference between the product gas and the surface of the QR , $T_g - T_s$, remains large. Therefore, the product gas can be quenched effectively by the QR. Two thermocouples were used to measure the product gas temperature before and after quenching. The first thermocouple (TC1) was installed near the QR tip to measure the pre-quenched gas temperature, and the second thermocouple (TC2) was installed above the QR to measure the gas temperature after quenching. Since the thermocouples were installed away from the central line of the reactor, the measured temperature does not represent the actual temperature of the product gas; nevertheless, it is possible to see

whether the QR functions appropriately. The measured temperatures at TC1 and TC2 at different CH_4/CO_2 ratios and SEI are shown in Fig. 2. Other details of the reactor configuration are shown in Fig. 1 below.

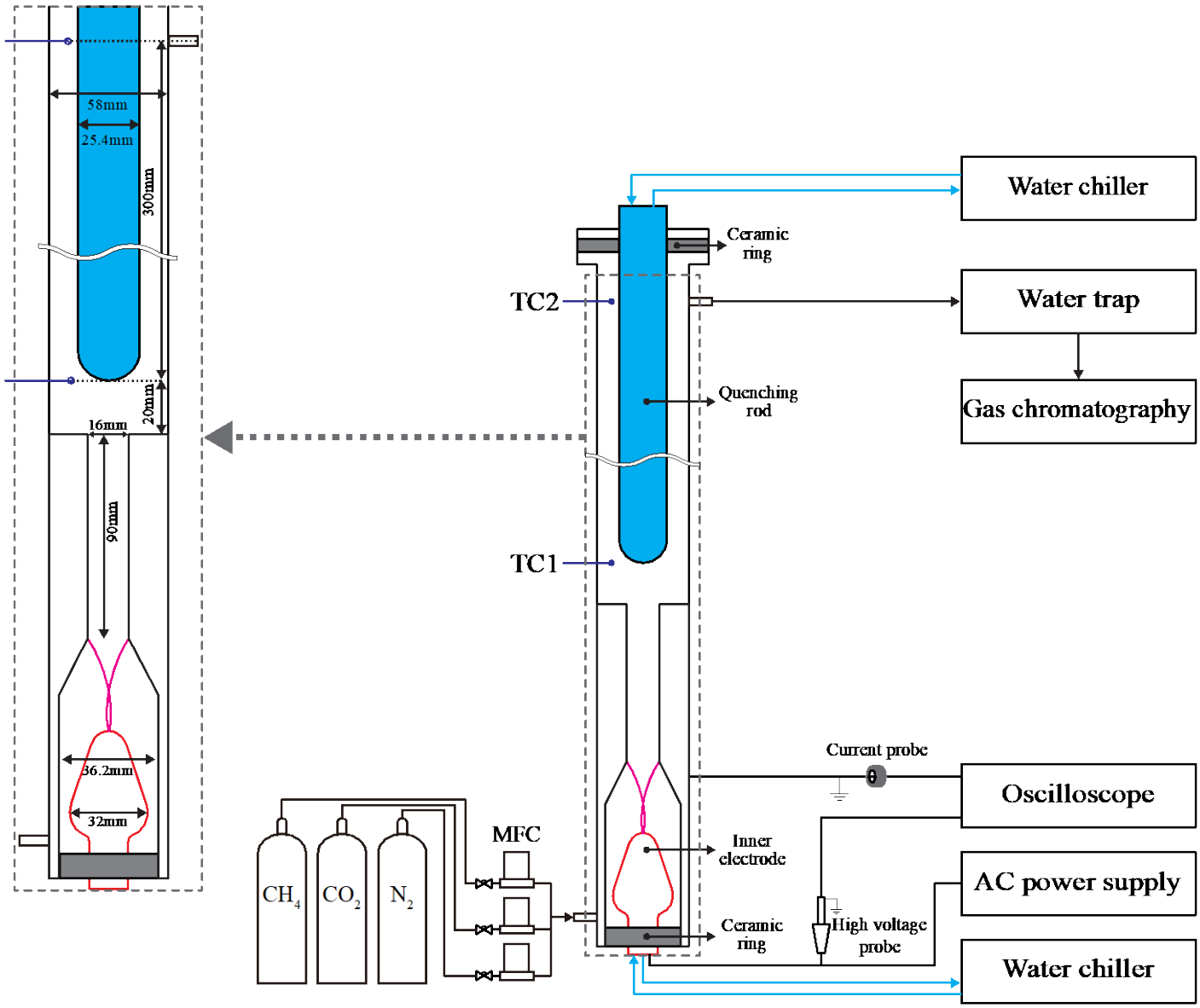

Fig. 1. Schematic of rotating gliding arc plasma system.

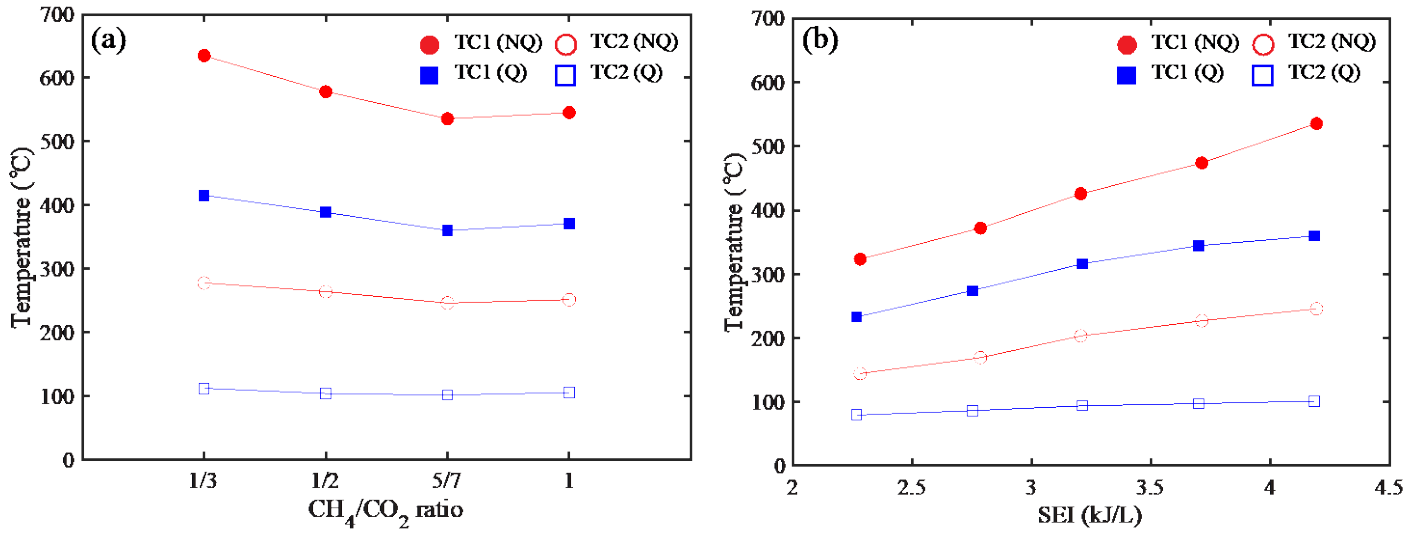

Fig. 2. Downstream gas temperature measured by TC1 and TC2 as a function of (a) CH_4/CO_2 ratio and (b) SEI. Red and blue markers represent data of not-quenched (NQ) and quenched (Q) experiments.

2.2. Experimental setup

The AC plasma power supply was connected to the inner electrode, and the external electrode was grounded. Arc discharge was driven by a power supply that can provide up to 2 kW power with a voltage of several kV and a current of several hundred mA. An oscilloscope (TBS2000, Tektronix) was used to collect electrical data delivered to the reactor. The arc discharge voltage and current data were obtained with a high-voltage probe (P6015A, Tektronix) and a current probe (TCP0150, Tektronix). The plasma power was calculated by integrating the product of the voltage and current over time, as described in (E2). Fig. 3 illustrates an example of waveforms of the discharge voltage and current at an input power set value of 1800 W and 20 kHz.

$$P_{plasma} = \frac{1}{T}\int V \cdot I \ (Watt) \qquad (E2)$$

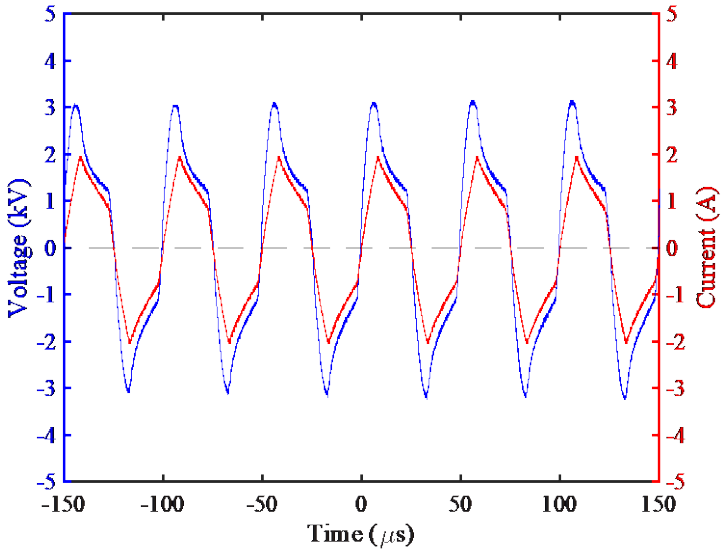

Fig. 3. Waveforms of discharge voltage and current at an input power set value of 1800 W and with a CH_4/CO_2 ratio of 5/7 over the period of 300 μs.

A mixture containing CH_4 and CO_2 (99.999% purity) as reactants and N_2 (99.999% purity) as an admixture useful for increasing the gas temperature and promoting arc stabilization was injected as the feed gas. Its flow rate was controlled by a mass flow controller (MFC, FC-2902, Mykrolis). Subsequently, the mixture of four different CH_4/CO_2 ratios (i.e., 1/3, 1/2, 5/7, and 1) was injected while the N_2 flow rate and total flow rate were kept at 12 and 24 SLPM, respectively.

The experiments were performed through the following procedure. First, the inside of the reactor was flushed for 5 min by injecting feed gas before arc ignition. To sample product gas under constant conditions, the reactor was heated up and the arc discharge operation was stabilized for 10 min after the power supply had been turned on. Finally, to remove deposited carbon from the electrodes, CO_2 was supplied for 3 min while the power supply was turned on. This procedure was repeated three times for each experiment case. CH_4, CO_2, CO, H_2, N_2, H_2O, and C_2H_2 were detected as the main product gases, and small amounts of C_2H_4 and C_2H_6 were detected. In addition, no C_3 hydrocarbons were detected. After removing H_2O through a water trap, the product gas was analyzed by a gas chromatograph (GC, 7890B, Agilent), which was calibrated for the gases CH_4, CO_2, N_2, O_2, H_2, CO, C_2H_2, C_2H_4, C_2H_6, and C_3H_8; it has two detectors (i.e., TCD and FID).

The definitions to evaluate the DRM performance were determined as follows:

The (absolute) conversion of the reactant *i* (either CH_4 or CO_2) is as follows:

$$\mathrm{X}_i = \frac{c_i^{in} - \alpha \cdot c_i^{out}}{c_i^{in}} \cdot 100\ (\%), \tag{E3}$$

where c_i^{in} and c_i^{out} are the concentrations of the reactants measured without and with plasma, respectively. And α is a correction factor that accounts for gas expansion during the DRM process, it is presented in (E4).

$$\alpha = \frac{c_{\mathrm{N}_2}^{in}}{c_{\mathrm{N}_2}^{out}}, \tag{E4}$$

where $c_{\mathrm{N}_2}^{in}$ and $c_{\mathrm{N}_2}^{out}$ represent the concentrations of N_2 without and with plasma, respectively. The (absolute) conversion is simply named "conversion" in the remainder of this paper.

The total conversion, which is the weighted average of the conversion of each reactant, is defined in (E5). The total conversion is necessary to consider the dilution effect of CH_4 and CO_2 in N_2, and to calculate the conversion cost, which will be defined below.

$$\mathrm{X}_{tot} = \sum_i c_i^{in} \cdot \mathrm{X}_i \cdot 100\ (\%) \tag{E5}$$

The selectivity and yield of product *j* in terms of *a*-atoms were calculated with (E6) and (E7), respectively. In this work, only H_2, CO, H_2O, and C_xH_y were considered as product *j*.

$$S_{j,a} = \frac{\mu_{j,a} \cdot \alpha \cdot c_j^{out}}{\sum_i \mu_{i,a} \cdot \left(c_i^{in} - \alpha \cdot c_i^{out}\right)} \cdot 100\ (\%), \tag{E6}$$

$$Y_{j,a} = \frac{\mu_{j,a} \cdot \alpha \cdot c_j^{out}}{\sum_i \mu_{i,a} \cdot c_i^{in}} \cdot 100\ (\%), \tag{E7}$$

where the coefficients $\mu_{i,a}$ and $\mu_{j,a}$ are the amounts of *a*-atoms in reactant *i* and product *j*, respectively.

The energy efficiency of the DRM process is defined as follows:

$$\eta = \frac{\alpha \cdot \left(\sum_j c_j^{out} \cdot \mathrm{LHV_j}\right)}{SEI + \sum_i \left(c_i^{in} - \alpha \cdot c_i^{out}\right) \cdot \mathrm{LHV}_i} \cdot 100\ (\%), \tag{E8}$$

where LHV_j (kJ/L) in the dividend of (E8) is the lower heating value of product *j*; only the LHV of the syngas (i.e., H_2 and CO) was considered owing to small amounts of C_xH_y. In addition, SEI (kJ/L) is the specific energy input:

$$\mathrm{SEI} = \frac{\mathrm{P}_{plasma} \cdot 60}{\text{Total flow rate}}\ (\mathrm{kJ/L}), \tag{E9}$$

where P_{plasma} is the plasma power calculated with (E2); the total flow rate was 24 SLPM in all experiments.

The energy costs for the required energy for the reactant conversion (i.e., the conversion cost) and syngas production (i.e., the syngas cost) are defined in (E10) and (E11), respectively:

$$\text{Conversion Cost} = \frac{\text{SEI}}{X_{tot}} \text{ (kJ/L)}, \tag{E10}$$

$$\text{Syngas Cost} = \frac{\text{SEI} \cdot \sum_i c_i^{in}}{\alpha \cdot \sum_j c_j^{out}} \text{ (kJ/L)}. \tag{E11}$$

The H_2/CO ratio of the syngas is defined as follows:

$$H_2/CO = \frac{c_{H_2}^{out}}{c_{CO}^{out}}, \tag{E12}$$

where $c_{H_2}^{out}$ and c_{CO}^{out} are the concentrations of H_2 and CO with plasma, respectively.

3. Results and Discussion

3.1 Thermodynamic equilibrium analysis

Since the strategy used in this study is to increase the selectivity and yield of H_2 by controlling the RWGS reaction by quenching the high-temperature product gas downstream of the reactor, thermodynamic equilibrium analysis of DRM is helpful to obtain insight into the influence of RWGS reaction on the conversion of the reactants (i.e., CH_4 and CO_2) and the yield of the products (i.e., H_2, CO, H_2O, and C(s)) for the DRM processes.

The equilibrium analysis of DRM was conducted with the HSC Chemistry 5.0 software with a Gibbs free energy minimization algorithm. Fig. 4 shows the equilibrium composition for DRM as a function of the temperature (500–2000 K) and different CH_4/CO_2 ratios: (a) 1/2, (b) 5/7, (c) 1, and (d) 7/5 at 1 atm. CH_4, CO_2, H_2, CO, H_2O, and C(s) were considered the main products of the DRM process. First, the thermodynamic equilibrium calculation for the DRM process was analyzed by focusing on the conversion of CH_4 and CO_2. The conversion of CH_4 is higher than that of CO_2 for all CH_4/CO_2 ratios. This indicates that CH_4 can be decomposed with less thermal energy than CO_2 owing to the strong bond energy of CO_2. Meanwhile, CO_2 was rapidly converted as the CH_4/CO_2 ratio increased (from Fig. 4(a) to (d)). This is due to the fact that adding the reducing agent CH_4 causes CH_4 to react with O atoms and O_2 molecules from CO_2 decomposition, thereby preventing CO from recombining into CO_2. At a high CH_4/CO_2 ratio, as there are fewer opportunities for CH_4 to react with O atoms and O_2 molecules, CH_4 and CO_2 are mainly converted via DRM, and the excessive CH_4 amount is decomposed into H_2 and C_2 hydrocarbons via dehydrogenation (in reaction R3) [27, 29]. Hence, to achieve a high conversion efficiency in the DRM processes, a high CH_4/CO_2 ratio should be used to achieve a high conversion of CO_2. However, when the CH_4/CO_2 ratio exceeds 1 (Fig. 4(d)), carbon deposition occurs even at high temperatures (above 1500 K), thereby hindering the stable operation of RGA plasma. Therefore, conditions close to the stoichiometric condition should result in a higher conversion of the reactants and stable operation.

$$CH_4 \rightarrow 0.5C_2H_x + (2-0.25x)H_2 \text{ (x=2, 4, or 6)} \tag{R3}$$

In the next step, the results of the thermodynamic equilibrium calculation for DRM were analyzed in terms of the yield of the products. The yield of the products exhibits a notable trend. When the temperature is high (above approximately 1200 K) and the CH_4/CO_2 ratio is less than 1 (Fig. 4(a) and (b)), the equilibrium composition of CO_2 and H_2 decreases, and that of CO and H_2O increases. While, when the temperature is above 1200 K and the CH_4/CO_2 ratio is above 1 (Fig. 4(c) and (d)), the yield of H_2 increases, and almost no water is produced. These trends in a temperature range above 1200 K with different CH_4/CO_2 ratios can be elucidated based on the RWGS reaction (R2) [27].

The Gibbs free energy change of a reaction (ΔG) and equilibrium constant (K) can be calculated with (E13) and (E14), respectively:

$$\Delta G = \Delta H - T\Delta S, \tag{E13}$$

where ΔH and ΔS are the enthalpy change of a reaction and the entropy change of a reaction, respectively, and T is the absolute temperature in Kelvin.

$$K = \exp(-\Delta G/RT), \tag{E14}$$

where R is the gas constant ($8.314\ J/K \cdot mol$). From the thermodynamic definitions, the negative Gibbs free energy change of a reaction (ΔG) means that

the reaction is spontaneous, and the equilibrium constant (K) determines the extent of the spontaneity of the reaction. As shown in Fig. 5, the RWGS reaction has a negative (ΔG) value, and an increasing K above approximately 1100 K; thus, the RWGS reaction is more favored at a higher temperature. In addition, at a low CH_4/CO_2 ratio, surplus CO_2 can participate more in the RWGS reaction, thereby resulting in the RWGS reaction tending to shift toward the products (i.e., CO and H_2O). Therefore, the low yield of H_2 and the relatively high yield of H_2O at a high temperature and at a low CH_4/CO_2 ratio (Fig. 4(a) and (b)) are attributed to the RWGS reaction.

Indeed, for DRM in RGA plasma, the gas temperature after plasma conversion is sufficient for DRM and RWGS to take place simultaneously. Under these conditions, the RWGS reaction can be suppressed if the gas temperature is rapidly lowered with the QR; consequently, although there will be some decreases in the conversion of CO_2 and yield of CO, it is expected that a high yield of H_2 can be obtained. Moreover, this quenching effect will be reinforced at high temperatures and low CH_4/CO_2 ratios where RWGS reaction is more likely to occur.

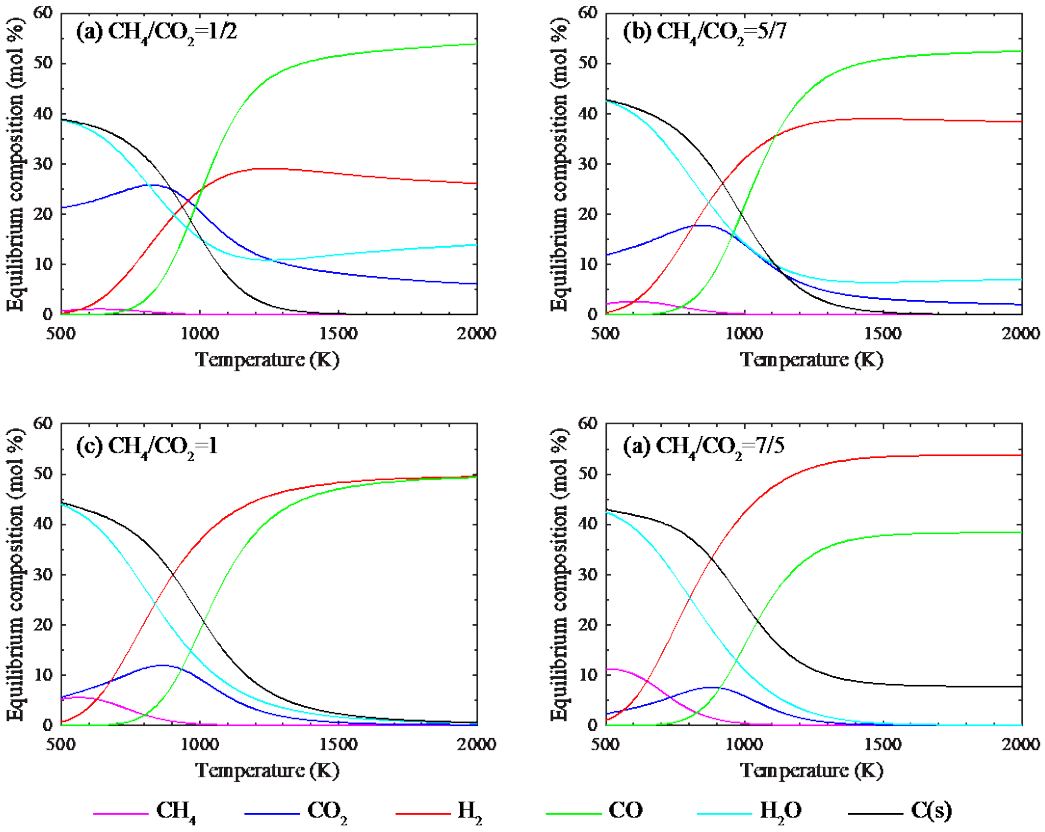

Fig. 4. Thermodynamic equilibrium composition for DRM as a function of temperature for CH_4/CO_2 ratios of (a) 1/2, (b) 5/7, (c) 1, and (d) 7/5 at 1 atm (HSC Chemistry 5.0 software with Gibbs free energy minimization algorithm)

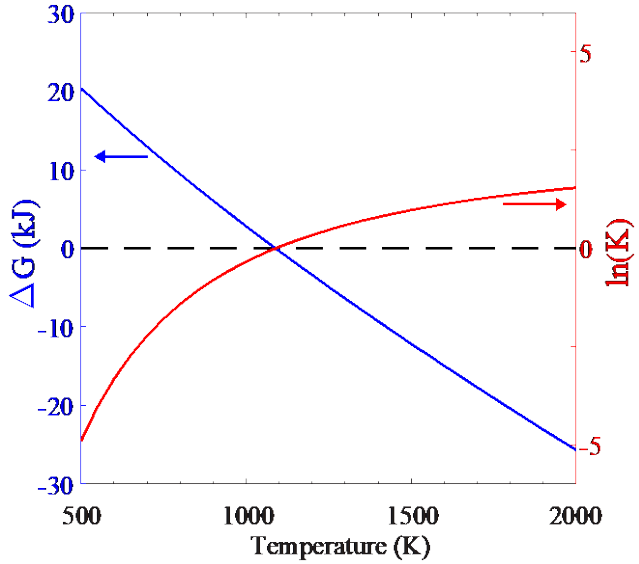

Fig. 5. Gibbs free energy change (blue) and equilibrium constant (red) of RWGS reaction as function of temperature.

3.2. Effect of quenching at different CH_4/CO_2 ratios

To evaluate the effect of quenching at different CH_4/CO_2 ratios, the QR was implemented downstream of the RGA reactor, and four CH_4/CO_2 ratios (i.e., 1/3, 1/2, 5/7, and 1) were tested at an input power set value of 1800 W. The N_2 flow rate (12 SLPM) and the total flow rate (24 SLPM) were maintained constant. Fig. 6 shows the conversion of the reactants as a function of the CH_4/CO_2 ratio. The conversion of CH_4 and CO_2 is represented by bars on the left y-axis. The conversion of CH_4 is represented by red (for not-quenched (NQ) experiments) and blue (for quenched (Q) experiments) bars; the conversion of CO_2 is shown as orange (NQ) and sky-blue (Q) bars. The total conversion is represented by red circles (NQ) and blue squares (Q) on the right y-axis**.** As shown in Fig. 6, the conversion of CH_4 was higher than that of CO_2 for all CH_4/CO_2 ratios as the bond dissociation energy for a C–H bond (4.48 eV) is lower than a C=O bond (5.52 eV) [24, 26]. For the NQ experiments, the conversion of CH_4 significantly decreased from 65.3% to 50.9% with increasing CH_4/CO_2 ratio, while the conversion of CO_2 had a maximum of 42.4% at a CH_4/CO_2 ratio of 1/2 and remained almost unchanged across the investigated CH_4/CO_2 ratios. This implies that the conversion of CH_4 is strongly affected by the CH_4/CO_2 ratio; at a high CH_4/CO_2 ratio where O_2 molecules and O atoms from CO_2 decomposition are depleted owing to low CO_2 concentration, CH_4 was converted through endothermic reactions such as DRM and dehydrogenation (R3) rather than oxidation reactions, thereby decreasing the conversion of CH_4 with increasing CH_4/CO_2 ratio. These trends in the conversion of the reactants are consistent with those presented in previously published studies [17, 18]. Combining the significant change in the conversion of CH_4 and the almost constant conversion of CO_2, the total conversion decreased with the CH_4/CO_2 ratio.

When the QR was applied (blue and sky-blue bars), the conversion of CH_4 and CO_2 was reduced. Moreover, the difference between not using and using the QR for the conversion of both CH_4 and CO_2 (i.e., the difference between red and blue bars and between orange and sky-blue bars) decreased with increasing CH_4/CO_2 ratio. Accordingly, the difference between not using and using the QR for the total conversion (i.e., the difference between red circles and blue squares) decreased with the CH_4/CO_2 ratio. This is because the product gas was quenched such that thermal conversions of CO_2 and CH_4 (reactions (R3–6)) [12, 22-24, 26] were suppressed. More specifically, the reaction (R4) plays an important role in the thermal conversion of CO_2 for the DRM processes, subsequently, the OH radicals produced via the reaction (R4) participate in the consumption of CH_4 and H_2 via the reactions (R6) and (R7) [12, 22-24, 26]. Therefore, when the QR was applied, the reaction (R4) was more effectively suppressed at the low CH_4/CO_2 ratio, which is rich in CO_2 to be converted through the reaction (R4), than at the high CH_4/CO_2 ratio; as a result, the larger difference between not using and using the QR for the conversion was observed at the low CH_4/CO_2 ratio than at the high CH_4/CO_2 ratio. For instance, by adding quenching at a CH_4/CO_2 ratio of 1/3, the total conversion decreased by 3.2% (from 23.4% to 22.6%), whereas, at a CH_4/CO_2 ratio of 1, the total conversion decreased by only 0.8% (from 22.7% to 22.5%).

$$CO_2+H\rightarrow CO+OH \quad (R4)$$

$$CH_4+H\rightarrow CH_3+H_2 \quad (R5)$$

$$CH_4+OH\rightarrow CH_3+H_2O \quad (R6)$$

$$H_2+OH\rightarrow H+H_2O \quad (R7)$$

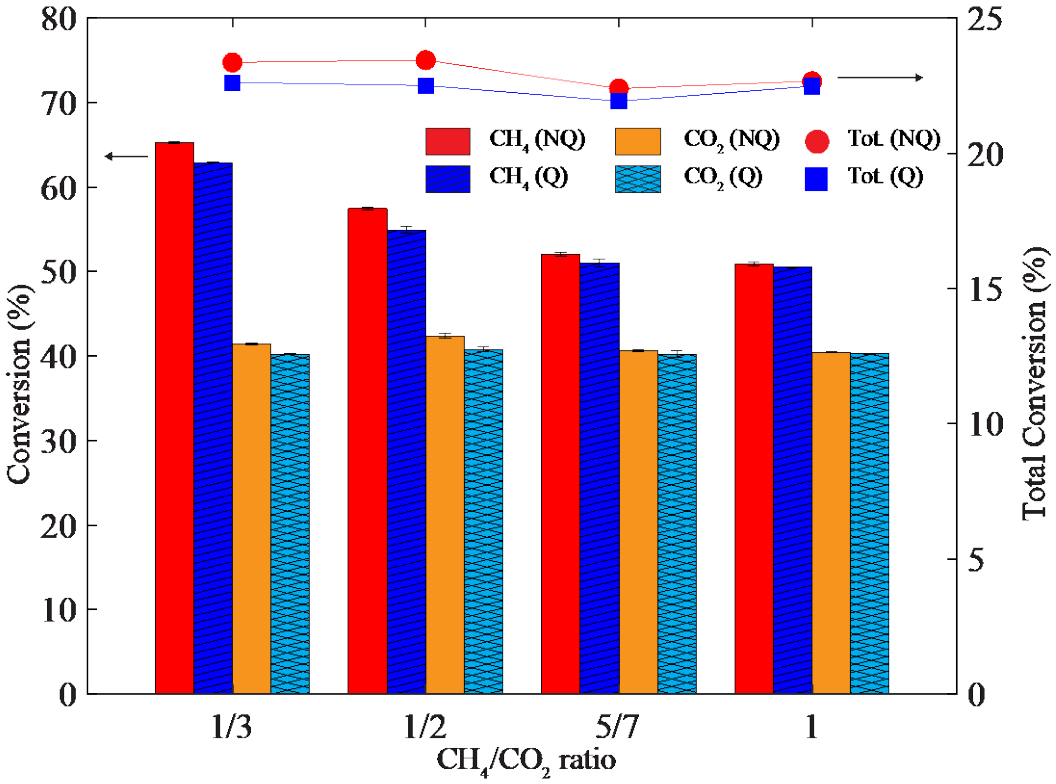

Fig. 6. Conversion of CH_4 and CO_2 and total conversion as functions of CH_4/CO_2 ratio. The conversion of CH_4 and CO_2 is represented by bars (left y-axis), and the total conversion (right y-axis) is presented with markers. The solid bars represent the conversion of not-quenched (NQ) experiments, and the patterned bars represent the conversion of quenched (Q) experiments. The error bars of three experimental results were added; however, they are often too small to be visible.

The selectivity and yield are presented as functions of the CH_4/CO_2 ratio in Fig. 7. The products (H_2, CO, H_2O, and C_2H_2) of the experiments without the QR are represented by red, orange, and yellow solid bars; for the experiments with the QR, the products are represented by blue, sky-blue, and yellow patterned bars. C_2H_4 and C_2H_6 were not considered because their concentrations were very low (i.e., about a few ppm). In addition, as H_2O could not be measured with the GC, the selectivity and yield of H_2O were calculated using the method presented in Pinhao's work [44]; see the detailed calculations in the Supplementary Material section (S1). By definition, the sum of all selectivities for each atom (C, H, and O) should be 100% when all products are considered. Similarly, the sum of all yields for each atom should be equal to the conversion of the reactants. For example, the sum of the H- and O-based yields should be equal to the conversion of CH_4 and CO_2, respectively, and the sum of the C-based yield should be equal to the total conversion. Indeed, the calculated sums of the H- and O-based selectivities are very close to 100%. However, owing to carbon deposition, the sum of the C-based selectivity

decreased from 100% to 97% with increasing CH_4/CO_2 ratio. The calculated sums of all C-, H-, and O-based yields were very close to the total, CH_4, and CO_2 conversion, respectively.

The trends of the selectivity of CO (red and blue bars in Fig. 7(a)) and that of C_2H_2 (yellow bars in Fig. 7(a)) were opposite in the experiments; the decrease in the selectivity of CO with increasing CH_4/CO_2 ratio is attributed to the increase in the selectivity of C_2H_2. This is because, as aforementioned in section 3.1, more C_2 hydrocarbons were formed via reaction (R3) at a high CH_4/CO_2 ratio. While the selectivity of H_2 (red and blue bars in Fig. 7(b)) and H_2O (orange and sky-blue bars in Fig. 7(b)) showed opposite trends; the selectivity of H_2 increased with increasing CH_4/CO_2 ratio, whereas the H_2O selectivity decreased with increasing CH_4/CO_2 ratio. From the trend in H-based selectivity, it can be inferred that at a low CH_4/CO_2 ratio, which is rich in CO_2, DRM was accompanied by the RWGS reaction, thereby resulting in the lower selectivity of H_2 and higher selectivity of H_2O; conversely, a higher selectivity of H_2 and a lower selectivity of H_2O at a high CH_4/CO_2 ratio indicate that H_2 was mainly produced via the DRM reaction. For the NQ experiments, the C-based selectivity of CO (red bars in Fig. 7(a)) was in the range of 81.2% to 98.2% for all CH_4/CO_2 ratios, while the selectivity of C_2H_2 (yellow bars in Fig. 7(a)) was in the range of 3.1% to 16.1%. Meanwhile, the H-based selectivity of H_2 (red bars in Fig. 7(b)) was in the range of 53.2% to 83.5%, which is relatively low compared to the C-based selectivity of CO, and the remaining H-based selectivity was occupied by H_2O (in the 45.4% to 8.6% range) and C_2H_2 (in the 2% to 7% range). These measured selectivities of the products were within the range of results from other studies [12, 17, 18, 21, 22, 24, 25]. In this regard, the relatively low selectivity of H_2 is why the QR is applied in the DRM processes; in this study, it was investigated whether the DRM performance could be improved with the high selectivity of H_2 by suppressing RWGS reaction through the QR.

For the quenching experiments, the C- and O-based yields of CO (blue bars in Fig. 7(a) and (c)) were reduced compared to those without the QR (red bars in Fig. 7(a) and (c)), while the selectivity of CO remained almost unchanged even with the QR. This reveals that CO was mainly produced by the CO_2 conversion rather than CH_4 conversion in proportion to the amount of converted CO_2, as the C-based CO selectivity, defined as the ratio of CO produced to the sum of CH_4 and CO_2 converted, was almost unchanged despite the decrease in the conversion of CH_4; therefore, as reported in other literature [10, 12], it can be deduced that the RWGS reaction is a major contributor for CO_2 conversion in the DRM processes. Meanwhile, the selectivity and yield of H_2 with the QR (blue bars in Fig. 7(b)) were higher than those without the QR (red bars in Fig. 7(b)). This is due to the fact that more H_2 was produced from the lower conversion of CH_4 with quenching (blue bars in Fig. 6) than from the higher conversion of CH_4 without quenching (red bars in Fig. 6); this means that the RWGS reaction was suppressed by the QR, thus H_2 being protected from conversion into H_2O via the RWGS reaction. Based on the literature [12], the elementary reactions $CO_2+H\rightarrow CO+OH$ (R4) and $H_2+OH\rightarrow H+H_2O$ (R7), which lead to the overall reaction $CO_2+H_2\rightarrow CO+H_2O$ (RWGS reaction (R2)), are the most dominant reactions for the reduction of CO_2 among the thermal reactions that occur during the DRM processes. Hence, it was confirmed that when the gas temperature was rapidly lowered by the QR, among the successive thermal reactions downstream of the reactor, the RWGS reaction was suppressed to a significant extent; indeed, since the QR effectively lowered the temperature of the product gas (Fig. 2) and suppressed RWGS reactions, the yield of CO (blue bars in Fig. 7(a) and (c)) decreased, and the selectivity and yield of H_2 (blue bars in Fig. 7(b)) increased. For the experiments with the QR at a CH_4/CO_2 ratio of 1, the H-based selectivity and yield of H_2 (blue bars in Fig. 7(b)) increased by 4.7% and 4%, thereby reaching the highest values (87.4% and 44%, respectively). At the same time, there were significant changes in the H-based selectivity and yield of H_2O; the selectivity of H_2O notably decreased by 46.9% (from 8.6% to 4.6%), and the yield of H_2O significantly decreased by 46.8% (from 4.3% to 2.3%). The changes in the selectivity and yield of H_2 and H_2O (Fig. 7(b)) confirm that the quenching method applied to protect H_2 from being converted into H_2O via thermal conversion, particularly via the RWGS reaction, functioned well.

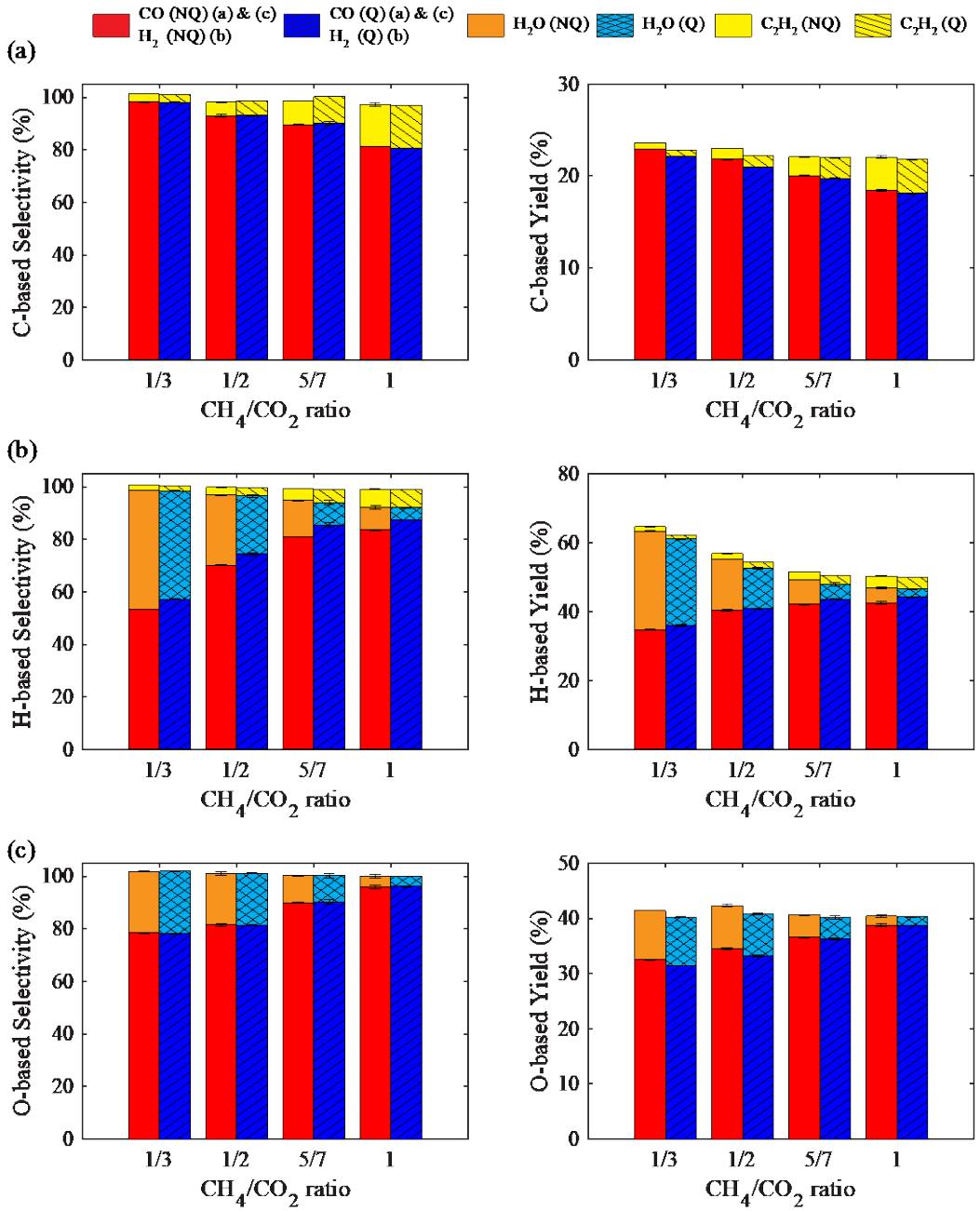

Fig. 7. (a) C-, (b) H-, and (c) O-based selectivities (left) and yields (right) as functions of CH_4/CO_2 ratio. Solid bars represent selectivities and yields for not-quenched (NQ) experiments, and patterned bars represent selectivities and yields for quenched (Q) experiments. The error bars of three experimental results were added; however, they are often too small to be visible.

To evaluate the effect of changes in the selectivities of products derived with the QR on the DRM performance, the energy efficiency (E8) and energy costs (E10, 11) were calculated. To consider the changes in the selectivity of H_2, the energy efficiency was calculated based on the lower heating values (LHV) instead of the reaction enthalpy. Fig. 8 illustrates the energy efficiency and energy costs as functions of the CH_4/CO_2 ratio. The conversion cost (Fig. 8(a)) and syngas cost (Fig. 8(b)) are represented by red (NQ) and blue (Q) bars on the left y-axis. The efficiency is represented by red circles (NQ) and blue squares (Q) on the right y-axis. As defined in (E10), the conversion cost is inversely proportional to the total conversion (see red circles and blue squares

in Fig. 6). For the NQ tests (red bars in Fig. 8(a)), the lowest conversion cost of 17.8 kJ/L was obtained at a CH_4/CO_2 ratio of 1/2, at which the total conversion had a maximum of 23.4%. When the QR was used, the conversion cost (blue bars) was higher than those of the NQ experiments; this is due to the fact that the total conversion was reduced (see blue squares in Fig. 6) as the thermal reactions such as reactions (R3–6) was suppressed. For instance, at a CH_4/CO_2 ratio of 5/7, the conversion cost increased from 18.7 kJ/L without the QR to 19.1 kJ/L with the QR.

Contrary to the negative impact of quenching on the conversion cost, quenching improved the energy efficiency at all CH_4/CO_2 ratios other than the CH_4/CO_2 ratio of 1/3 at which the same energy efficiency was obtained. This is due to the increase in H_2 production saved from conversion into H_2O via the RWGS reaction, thereby increasing the LHV of syngas (which is in the dividend of (E8)). Meanwhile, the increasing trend of the energy efficiency in the range of CH_4/CO_2 ratio from 1/3 to 5/7 was followed by a slight decrease at a CH_4/CO_2 ratio of 1; this is ascribed to the increased discharge instability induced by the carbon deposition on the electrodes at a CH_4/CO_2 ratio of 1 (the C-balance was 97% at a CH_4/CO_2 ratio of 1). In addition, as shown in Fig. 2(a), the gas temperature measured at TC1 showed a trend opposite to the energy efficiency; a slight increase in the gas temperature was observed between the CH_4/CO_2 ratio of 5/7 and 1. This means that energy was not efficiently used for the conversion owing to discharge instability induced by the carbon deposition, but rather was used for raising the gas temperature, thereby resulting in the lower energy efficiency at a CH_4/CO_2 ratio of 1.

The syngas cost decreased with increasing CH_4/CO_2 ratio regardless of the QR (red and blue bars in Fig. 8(b)); this trend is inversely proportional to the syngas yield, which is the sum of the H-based yield of H_2 and the O-based yield of CO. When the QR was used (blue bars), a higher syngas cost was obtained at low CH_4/CO_2 ratios of 1/3 and 1/2. However, this trend was reversed above a CH_4/CO_2 ratio of 5/7 with the QR; the resulting syngas cost was lower. When the CH_4/CO_2 ratio was 1, the syngas cost was lowest (10.2 kJ/L); however, the energy efficiency (53.2%) was lower than that (55.3%) at a CH_4/CO_2 ratio of 5/7. Despite the lowest syngas cost, at a CH_4/CO_2 ratio of 1, a substantial amount of carbon was deposited (i.e., the C-balance was 97% at a CH_4/CO_2 ratio of 1); this ratio would severely affect the long-term operation and is, thus, unsuitable for industrial application. Therefore, a CH_4/CO_2 ratio of 5/7, at which the highest energy efficiency (55.6%) and competitive syngas costs (10.9 kJ/L) were obtained, was selected as the ratio to investigate further the effect of quenching with different input power values.

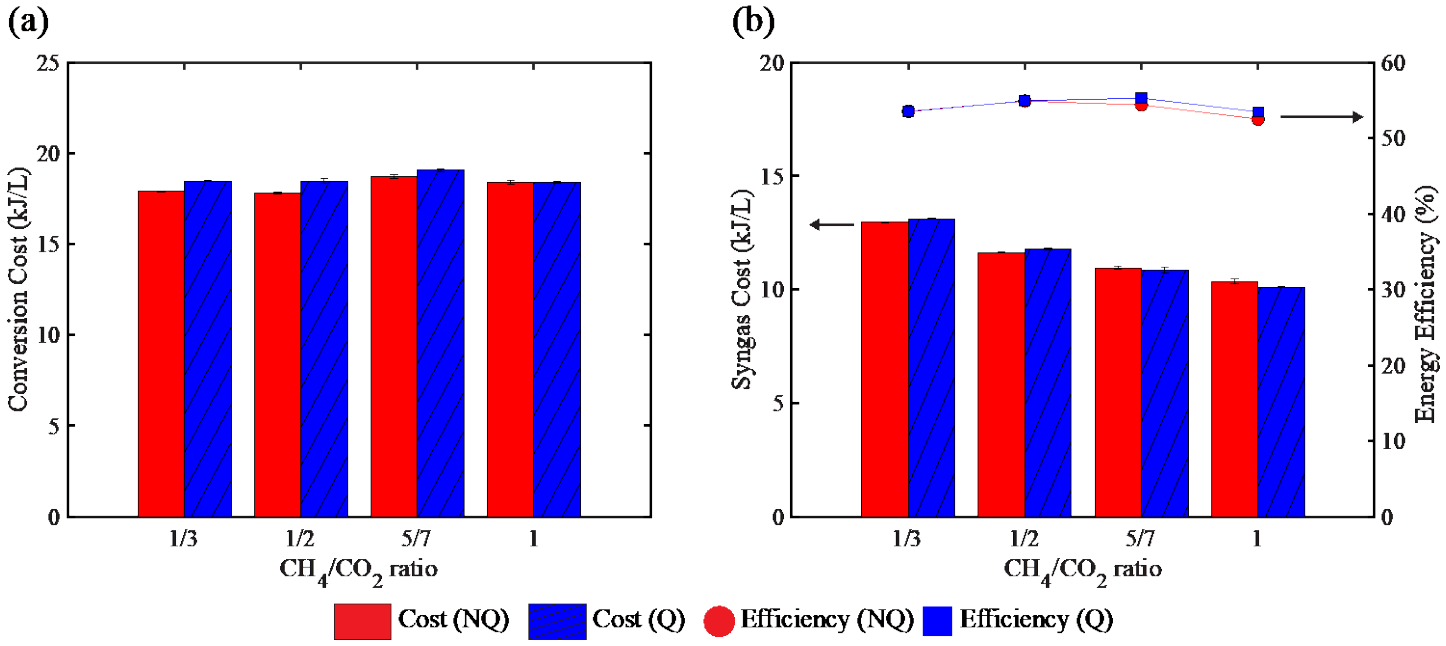

Fig. 8. Energy costs and energy efficiency as functions of CH_4/CO_2 ratio: (a) conversion cost, and (b) syngas cost (bars, left y-axis) and energy efficiency (markers, right y-axis). Red bars and markers represent energy costs and energy efficiency of not-quenched (NQ) experiments, and blue bars and markers represent quenched (Q) experiments. The error bars of three experimental results were added; however, they are often too small to be visible.

3.3. Effect of quenching at different SEI

To evaluate the effect of quenching on the DRM performance at a CH_4/CO_2 ratio of 5/7, the input power, as a plasma parameter, was changed. The input power set value was varied from 1000 to 1800 W, corresponding to an SEI of 2.5–4.5 kJ/L according to (E9), and was measured in SEI values of 2.3–4.2 kJ/L. Fig. 9 illustrates the conversion of the reactants (CH_4 and CO_2) and total conversion as functions of the SEI with and without the QR. Such as in the previous section, the red (NQ) and blue (Q) bars represent the conversion of CH_4, and the orange (NQ) and sky-blue (Q) bars represent the conversion of CO_2. In addition, the total conversion is represented by red circles (NQ) and blue squares (Q) on the right y-axis. The increase in the SEI leads to a high electron density. In this case, more electron collision-induced dissociation is initiated, and more thermal reactions take place owing to the increased gas temperature through VT relaxation; therefore, the gas temperature increased with increasing SEI (see Fig. 2(b)), consequently, the conversion of both CH_4 (red and blue bars) and CO_2 (orange and sky-blue bars) increased with the SEI. This trend is consistent with the experimental results presented in previously published studies [12, 18, 21]. In addition, owing to the rising trend of the conversion of CH_4 and CO_2, the total conversion increased with increasing SEI.

When the QR quickly cooled the product gas, the conversion of CH_4 (blue bars) and CO_2 (sky-blue bars) was reduced, thereby reducing the total conversion (blue squares). Meanwhile, as the SEI increased, the difference between using and not using the QR for the conversion increased with the SEI. This is because more CH_4 and CO_2 were converted through thermal conversion such as reactions (R3–6) with increasing temperature; hence, when the QR was applied at a high SEI, the thermal conversion was more effectively suppressed than at a low SEI, thereby resulting in a larger difference in the conversion between using and not using the QR at a high SEI. Furthermore, as mentioned in section 3.1, more RWGS reactions occurred with increasing temperature owing to the increasing K value, thus, it can be deduced that the quenching effect on suppressing the RWGS reaction was reinforced at a high SEI. As a result, when the QR was used, the total conversion slightly decreased by only 0.9% (from 11.2% to 11.1%) at a low SEI of 2.3 kJ/L, while the total conversion decreased by 2.1% (from 22.4% to 21.9%) at a high SEI of 4.2 kJ/L.

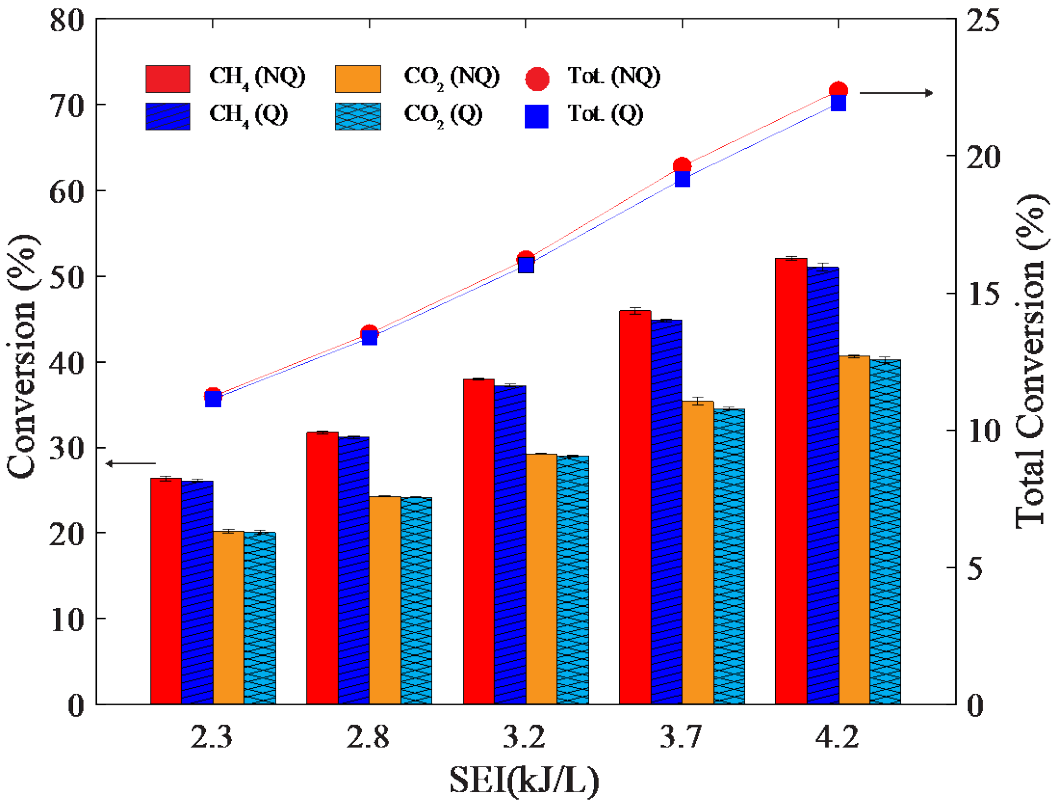

Fig. 9. Conversion of CH_4 and CO_2 and total conversion as functions of SEI. The conversion of CH_4 and CO_2 is represented by bars (left y-axis) and the total conversion (right y-axis) is represented by markers. Solid bars represent conversion of not-quenched (NQ) experiments, and patterned bars represent conversion of quenched (Q) experiments. The error bars of three experimental results were added; however, they are often too small to be visible.

Fig. 10 shows the selectivity and yield of the products as a function of the SEI. The selectivity and yield without the QR are represented by solid bars, and the selectivity and yield with quenching are represented by patterned bars. The sums of C-, H-, and O-based selectivities were very close to 100%, and almost no carbon was deposited at CH_4/CO_2 ratio. In addition, the calculated C-, H-, and O-based yields were close to the total, CH_4, and CO_2 conversion, respectively. For the experiments without the QR (red, orange, and yellow solid bars), the selectivities of all products remained constant across the investigated SEI range; this indicates a weak relationship between the input power and reaction pathways [9]. In addition, for the NQ experiments, the yields of all products increased with the SEI, which is attributed to the increase in the conversion of the reactants with increasing SEI. For the NQ experiments, the measured C-based selectivity of CO (red bars in Fig. 10(a)) was high (approximately 90%) across the investigated SEI range; the selectivity of C_2H_2 (yellow bars in Fig. 10(a)) was only approximately 9%. While the H-based selectivity of H_2 (red bars in Fig. 10(b)), which accounts for approximately 81% of the H-based selectivity, was not as high as the selectivity of CO, and the remaining 14% and 4.5% of the H-based selectivity were occupied by H_2O (orange bars in Fig. 10(b)) and C_2H_2 (yellow bars in Fig. 10(b)), respectively. Again, the result of the H-based selectivity, i.e., the relatively low H_2 selectivity compared to the CO selectivity and relatively high H_2O selectivity compared to the C_2H_2 selectivity, is the reason the quenching method is proposed in this study; to distribute H-atoms to H_2 rather than H_2O by suppressing the RWGS reaction with a quenching device.

For the same reason as explained in Fig. 7, since CO was mainly produced by the CO_2 conversion, the C- and O-based selectivity of CO remained nearly unchanged even with the QR; the C-based CO selectivity only increased by 1% owing to a decrease in the conversion of CH_4. In addition, when the QR was used, the yield of CO was reduced compared to that of the experiment without the QR; it decreased more at a high SEI. This implies that the RWGS reaction was more suppressed by the QR owing to the higher temperatures at a high SEI. By contrast, when the QR was used, the selectivity and yield of C_2H_2 increased with increasing SEI because the temperature was not high enough to overcome the strong C≡C bond. Moreover, this trend of the selectivity

of C_2H_2 is consistent with the results of plasma-based CH_4 conversion studies; the authors reported that a higher selectivity of C_2H_2 can be obtained by quenching the hot product gas from CH_4 pyrolysis [45, 46]. It should be noted that the increase in the yield of C_2H_2 had a negative effect on the quenching to increase the selectivity of H_2, but it was negligible because the yield of C_2H_2 was small (approximately 1–2% in the H-based selectivity).

Fig. 10(b) presents evident changes in both the H-based selectivity and yield for experiments with the QR. The selectivity and yield of H_2 with the QR (blue bars) were higher than without the QR (red bars), whereas the opposite trend was observed for H_2O (orange and sky-blue bars). Again, this results from the RWGS reaction being limited by the QR; thus, less CO_2 was converted into CO, and more H_2 was saved from the conversion into H_2O via the RWGS reaction. In addition, since the RWGS reaction is more likely to occur at high temperatures, applying the QR at a higher SEI could further suppress the RWGS reaction. Therefore, remarkable changes in the H-based selectivity and yield were observed at a high SEI for the quenching experiments; when the QR was applied at an SEI of 4.2 kJ/L, the selectivity and yield of H_2 increased by 5.5% and 3.4%, thereby reaching the highest values (85.4% and 43.6%, respectively). Conversely, the selectivity and yield of H_2O significantly decreased by 38% (from 13.9% to 8.6%) and by 38.6% (from 7.1% to 4.3%), respectively. Regarding the experimental results for the selectivity of the products, the selectivity of H_2 did not reach a value as high as that of CO (90.1% at an SEI of 4.2 kJ/L), but the quenching effect on the selectivity of H_2 (85.4% at an SEI of 4.2 kJ/L) was observed; moreover, the selectivity of H_2O (8.6% at an SEI of 4.2 kJ/L) was significantly reduced by quenching, thereby almost reaching the value of the C_2H_2 selectivity (5.1% at an SEI of 4.2 kJ/L); therefore, it is expected that further improvement of the H_2 selectivity can be achieved through optimization of the quenching method.

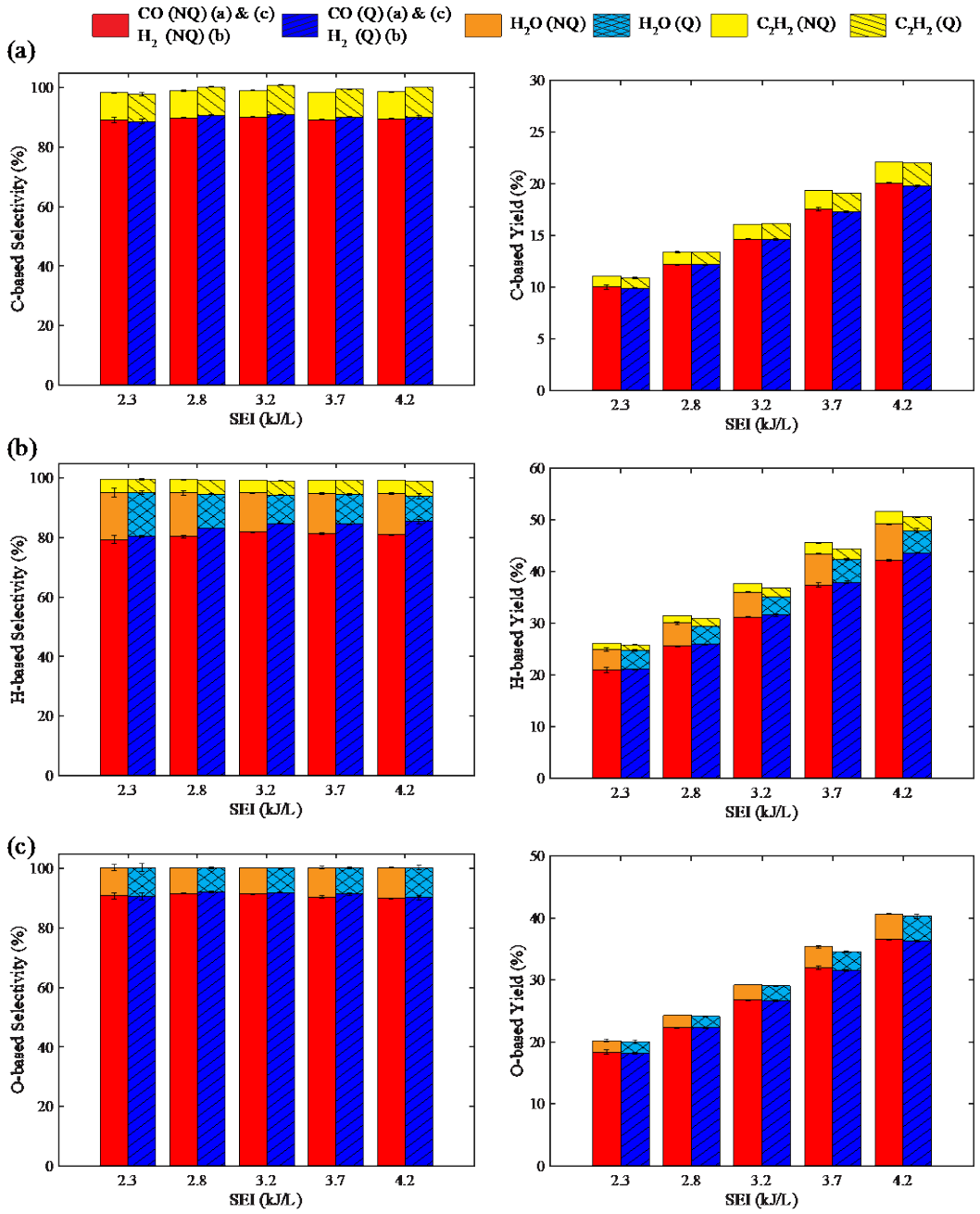

Fig. 10. (a) C-, (b) H-, and (c) O-based selectivities (left) and yields (right) as functions of SEI. Solid bars represent selectivities and yields of not-quenched (NQ) experiments, and patterned bars represent selectivities and yields of quenched (Q) experiments. The error bars of three experimental results were added; however, they are often too small to be visible.

The changes in the selectivity and yield of H_2 and H_2O prove that the strategy of distributing H-atoms to H_2 rather than H_2O by suppressing the RWGS reaction with a QR worked; thereby, resulting in a higher selectivity and yield of H_2. The changes in the selectivity and yield derived with the QR were reflected in the energy efficiency and energy costs. Fig. 11 illustrates the energy efficiency and energy cost as functions of the SEI. The description of Fig. 11 is similar to that of Fig. 8. The conversion and syngas costs decreased with increasing SEI since more CH_4 and CO_2 were converted, thereby resulting in higher yields of H_2 and CO with increasing SEI. In addition, the energy efficiency increased with the SEI owing to the increased LHV of the syngas.

When the QR was used, the RWGS reaction was suppressed, which reduced the total conversion (see Fig. 9); hence, the conversion costs (blue bars in Fig. 11(a)) were slightly higher than those without the QR (red bars in Fig. 11(a)). On the contrary, the syngas costs were lower (blue bars in Fig. 11(b)) since, when the gas was quenched, more H_2 was saved from conversion into H_2O even with the lower conversion of CH_4. In addition, as the LHV of the syngas increased owing to the higher yield of H_2, the efficiency was improved. When the QR was applied at an SEI of 4.2 kJ/L, the conversion cost increased from 18.7 to 19.1 kJ/L, whereas the syngas cost decreased to a minimum (10.9 kJ/L). Furthermore, the energy efficiency increased to the highest value (55.3%).

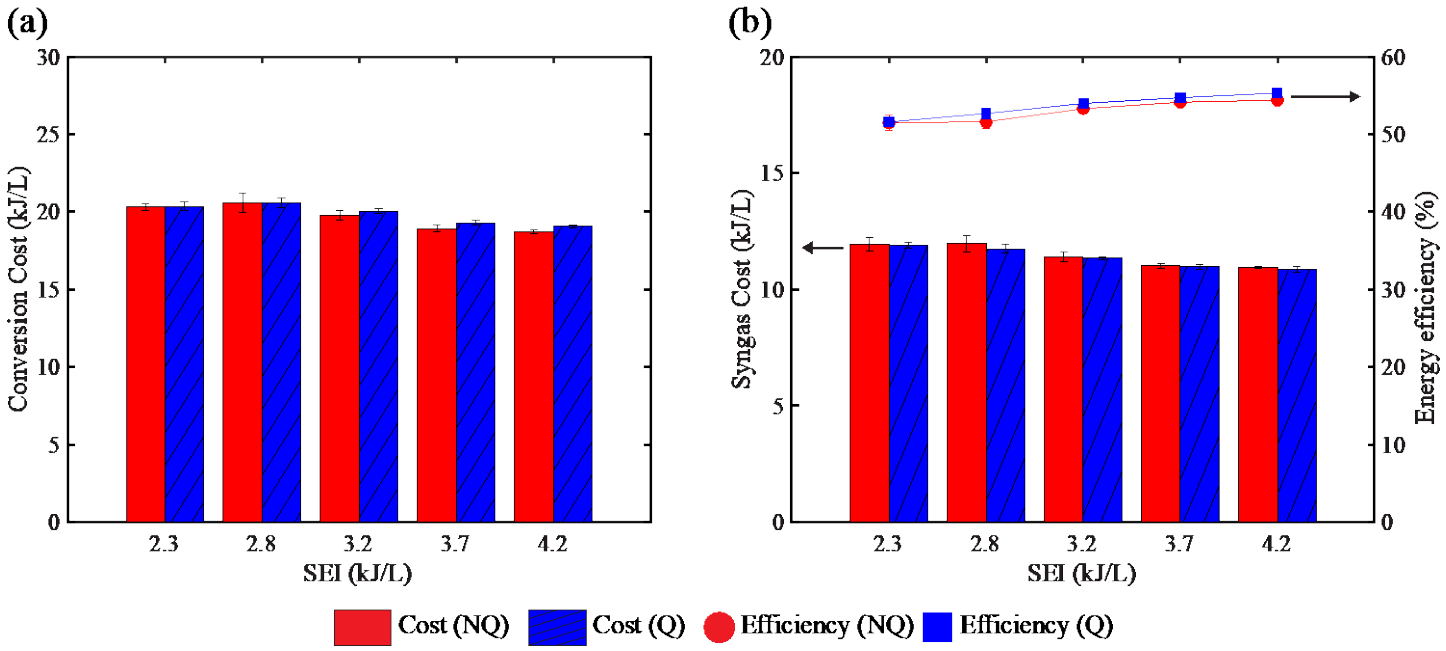

Fig. 11. Energy costs and energy efficiency as functions of SEI: (a) conversion cost, and (b) syngas cost (bars, left y-axis) and energy efficiency (markers, right y-axis). Red bars and markers represent energy costs and energy efficiency of not-quenched (NQ) experiments, and blue bars and markers represent quenched (Q) experiments. The error bars of three experimental results were added; however, they are often too small to be visible.

Meanwhile, to check the effect of the rod configuration on the reaction performance, an experiment using an empty rod (i.e., without cold water) was conducted at a CH_4/CO_2 ratio of 5/7 with an SEI of 4.2 kJ/L. When the empty rod was inserted, a stagnation point is formed, and the flow decelerates; hence, the gas temperature measured at TC1 slightly increased by about 25 ℃ compared to that of NQ case (536 ℃). In addition, both the surface area for heat dissipation and the velocity of the gas passing between the reactor wall and the rod increased by applying the rod; thus, the temperature measured at TC2 decreased by about 30 ℃ compared to that of NQ case (246 ℃). Nevertheless, since the temperature difference between the product gas and the empty rod surface was small without quenching (i.e., without cold water), the quenching effect on the gas temperatures was not observed (for quenching experiments, the temperatures at TC1 and TC2 were measured as 360 ℃ and 101 ℃, respectively). Consequently, when only the empty rod was used, the selectivity of H_2 (80.8%), H_2O (14.0%), and C_2H_2 (4.6%) were calculated close to those of NQ case (81%, 13.9%, and 4.6% for H_2, H_2O, and C_2H_2, respectively) as shown in Fig. 12; this indicates that the rod itself has little effect on the reaction pathway of DRM.

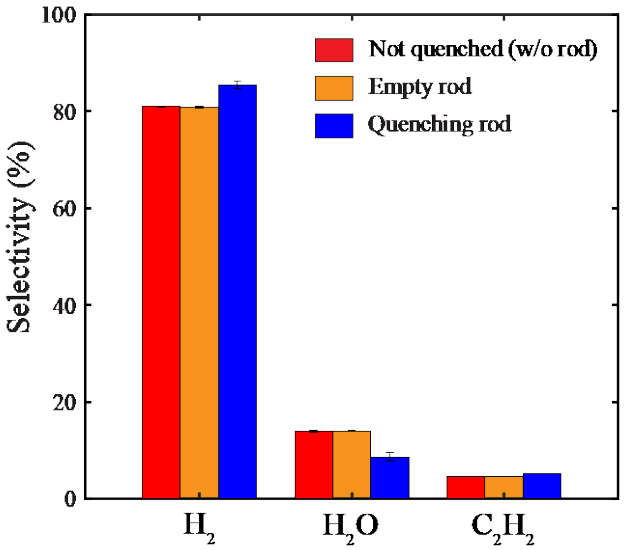

Fig. 12. The selectivity of H_2, H_2O, and C_2H_2: Red, orange, and blue bars represent the selectivity of not-quenched, empty rod, and quenching rod experiments, respectively. The error bars of three experimental results were added; however, they are often too small to be visible.

Table 1 compares the DRM performance for different RGA plasmas with similar CH_4/CO_2 ratios. The DRM performance obtained at a CH_4/CO_2 ratio of 5/7 was compared with that obtained at a CH_4/CO_2 ratio of 2/3. At a CH_4/CO_2 ratio of 5/7, the RGA reactor of this study achieved intermediate conversion of the reactants compared to that of other studies [17-19]. However, the energy costs were higher than those obtained by Liu et al. [17] and Dinh et al. [18]; unlike in those studies, using the N_2 admixture led to higher energy costs owing to the dilution effect of N_2. While, since the yield of H_2 was increased with the QR, the highest H_2/CO ratio (0.95) was achieved at a CH_4/CO_2 ratio of 5/7. Meanwhile, compared with the DRM performance of other works at a CH_4/CO_2 ratio of 1 [14, 16, 18, 22], intermediate conversion and energy costs were obtained, and the highest H_2/CO ratio (1.26) was achieved. Among the DRM studies using N_2, the GA plasmatron (GAP) [22] showed the best energy costs by achieving conversion costs of 11.3 kJ/L and syngas costs of 6.8 kJ/L, while the RGA reactor developed by Dinh et al. [21] showed the highest conversion of CH_4 and CO_2 (74% and 49%, respectively). In this study, the H_2/CO ratio was higher than those of other DRM studies using N_2, and the syngas cost (10.2 kJ/L) was lower than that presented by Dinh et al. [21]. Although the highest H_2/CO ratio was achieved using the RGA reactor with the QR, the best result was not obtained in terms of the energy costs. Regarding this, the authors believe there is room for further improvement in the energy cost through optimizing the quenching method; indeed, optimizing some parameters (such as length of the tubular outlet, QR tip position, and quenching rate) would enhance the quenching effect, thereby resulting in a higher H_2 selectivity and a lower syngas cost. Hence, optimization of the quenching method will be performed in our further research.

Table 1 Comparison of DRM performance of DRM processes in different RGA plasmas

Reactor type	$CH_4/CO_2/(N_2)$	SEI (kJ/L)	X_{CH_4} (%)	X_{CO_2} (%)	Conversion Cost [a] (kJ/L)	Syngas Cost [a] (kJ/L)	H_2/CO [a]	Reference
RGA	2/3	4.8	28.1	17	22.3	26	0.16	[19]
RGA	2/3	2.4	29	22	9.7	5.9	0.83	[17]
RGA	2/3	6.5	83	71	8.6	5.4	0.74	[18]
	1/1	6.5	75	65	9.3	5.1	1.17	
RGA	1/1	6.7	10.9	12.8	56.5	41.4	1.16	[14]

RGA	1/1	2.36	36	35	6.6	11.7	0.94	[16]
GAP	1/1/(2)	2.22 [b]	44.6 [b]	33.2 [b]	11.3	6.8	1.05	[22]
RGA	1/3/(4)	5	74	49	18.1	13.3	0.44	[21]
RGA	5/7/(12)	4.18	51.1	40.2	19.1	10.9	0.95 (0.91) [c]	This work
	1/1/(2)	4.17	50.5	40.3	18.5	10.2	1.26 (1.19) [c]	

[a] calculated with data from literature
[b] interpolated with data from literature
[c] H_2/CO ratio for NQ experiments

4. **Conclusions**

In this study, an RGA reactor was employed for DRM. The scope was to improve the efficiency and energy costs of DRM by increasing the selectivity and yield of desirable products, such as H_2 and CO. A QR was developed and applied downstream of the RGA reactor to suppress the RWGS reaction, which is dominant in the consumption of CO_2 and H_2 among the successive thermal reactions occurring in high-temperature downstream gas.

When the QR was applied, the conversion of CH_4 and CO_2 was reduced, while the selectivity and yield of H_2 increased over the entire range of investigated CH_4/CO_2 ratios. For the quenching experiments conducted at low CH_4/CO_2 ratios (1/3 and 1/2), the LHV of the syngas increased, which increased the energy efficiency. However, since the decrease in the conversion of the reactants induced by quenching outweighed the increase in the yield of H_2, both the conversion cost and syngas cost increased. When the QR was applied at high CH_4/CO_2 ratios (5/7 and 1), the trend of the syngas cost was reversed. At a CH_4/CO_2 ratio of 5/7, the highest energy efficiency (55.3%) and most competitive syngas costs (10.9 kJ/L) were attained with the QR at 51.1% and 40.2% conversion for CH_4 and CO_2, respectively. In addition, the experiments with different input powers confirmed that the effect of quenching on the DRM performance increased as the gas temperature increased, i.e., as the SEI increased. Compared with the results of other studies conducted at similar CH_4/CO_2 ratios, the highest H_2/CO ratios (0.95 and 1.26) were obtained with the QR at CH_4/CO_2 ratios of 5/7 and 1 in this study, respectively.

The results of this study demonstrate that by increasing the selectivity and yield of H_2 in the DRM processes through a QR, the efficiency and energy costs can be improved, and syngas with a high H_2/CO ratio can be produced. In addition, further improvement in the DRM performance is expected by optimizing the quenching method; hence, the quenching method can potentially be employed in the plasma-based DRM industry in the future.

Acknowledgments

This work was supported by the National Research Foundation of Korea (NRF) grant funded by the Korean Government (MSIT) (No. 2022R1A2B5B01002616).

References

[1] Q. Zhu, Developments on CO2-utilization technologies, Clean Energy 3(2) (2019) 85-100.
[2] Y.T. Shah, T.H. Gardner, Dry Reforming of Hydrocarbon Feedstocks, Catal Rev 56(4) (2014) 476-536.
[3] L.W. Chen, P. Gangadharan, H.H. Lou, Sustainability assessment of combined steam and dry reforming versus tri-reforming of methane for syngas production, Asia-Pac J Chem Eng 13(2) (2018).
[4] P.M. Maitlis, A.d. Klerk, Greener Fischer-Tropsch processes for fuels and feedstocks, Wiley-VCH, Weinheim, Germany, 2013, pp. 1 online resource (xviii, 372 pages).
[5] A.M. Ranjekar, G.D. Yadav, Dry reforming of methane for syngas production: A review and assessment of catalyst development and efficacy, J Indian Chem Soc 98(1) (2021).
[6] S.B. Wang, G.Q.M. Lu, G.J. Millar, Carbon dioxide reforming of methane to produce synthesis gas over metal-supported catalysts: State of the art, Energy Fuels 10(4) (1996) 896-904.
[7] S. Arora, R. Prasad, An overview on dry reforming of methane: strategies to reduce carbonaceous deactivation of catalysts, Rsc Adv 6(110) (2016) 108668-108688.
[8] A. Fridman, Plasma chemistry, Cambridge university press2008.

[9] R. Snoeckx, A. Bogaerts, Plasma technology - a novel solution for CO2 conversion?, Chem. Soc. Rev. 46(19) (2017) 5805-5863.
[10] A. George, B.X. Shen, M. Craven, Y.L. Wang, D.R. Kang, C.F. Wu, X. Tu, A Review of Non-Thermal Plasma Technology: A novel solution for CO2 conversion and utilization, Renew Sust Energ Rev 135 (2021).
[11] A. Bogaerts, E.C. Neyts, Plasma Technology: An Emerging Technology for Energy Storage, Acs Energy Lett 3(4) (2018) 1013-1027.
[12] J.L. Liu, Y. Gao, B. Sun, B. Zhu, X.S. Li, A.M. Zhu, Mechanism study on gliding arc (GA) plasma reforming: A combination approach of experiment and modeling, Plasma Process. Polym. (2022).
[13] H. Zhang, L. Li, X.D. Lia, W.Z. Wang, J.H. Yan, X. Tu, Warm plasma activation of CO2 in a rotating gliding arc discharge reactor, J Co2 Util 27 (2018) 472-479.
[14] J. Martin-del-Campo, S. Coulombe, J. Kopyscinski, Influence of Operating Parameters on Plasma-Assisted Dry Reforming of Methane in a Rotating Gliding Arc Reactor, Plasma Chem. Plasma Process. 40(4) (2020) 857-881.
[15] Y. Wang, Y. Chen, J. Harding, H. He, A. Bogaerts, X. Tu, Catalyst-free single-step plasma reforming of CH4 and CO2 to higher value oxygenates under ambient conditions, Chem. Eng. J. 450 (2022) 137860.
[16] A. Wu, J. Yan, H. Zhang, M. Zhang, C. Du, X. Li, Study of the dry methane reforming process using a rotating gliding arc reactor, Int. J. Hydrog. Energy 39(31) (2014) 17656-17670.
[17] J.L. Liu, H.W. Park, W.J. Chung, D.W. Park, High-Efficient Conversion of CO2 in AC-Pulsed Tornado Gliding Arc Plasma, Plasma Chem. Plasma Process. 36(2) (2016) 437-449.
[18] D.K. Dinh, S. Choi, D.H. Lee, S. Jo, K.-T. Kim, Y.-H. Song, Energy efficient dry reforming process using low temperature arcs, Plasma Process. Polym. 15(5) (2018) 1700203.
[19] N. Lu, D. Sun, Y. Xia, K. Shang, B. Wang, N. Jiang, J. Li, Y. Wu, Dry reforming of CH4CO2 in AC rotating gliding arc discharge: Effect of electrode structure and gas parameters, Int. J. Hydrog. Energy 43(29) (2018) 13098-13109.
[20] W. Wang, R. Snoeckx, X. Zhang, M.S. Cha, A. Bogaerts, Modeling Plasma-based CO2 and CH4 Conversion in Mixtures with N2, O2, and H2O: The Bigger Plasma Chemistry Picture, The Journal of Physical Chemistry C 122(16) (2018) 8704-8723.
[21] D.K. Dinh, G. Trenchev, D.H. Lee, A. Bogaerts, Arc plasma reactor modification for enhancing performance of dry reforming of methane, J Co2 Util 42 (2020).
[22] S. Van Alphen, J. Slaets, S. Ceulemans, M. Aghaei, R. Snyders, A. Bogaerts, Effect of N-2 on CO2-CH(4)conversion in a gliding arc plasmatron: Can this major component in industrial emissions improve the energy efficiency?, J Co2 Util 54 (2021).
[23] L. Zhang, S. Heijkers, W.Z. Wang, L.M. Martini, P. Tosi, D.Z. Yang, Z. Fang, A. Bogaerts, Dry reforming of methane in a nanosecond repetitively pulsed discharge: chemical kinetics modeling, Plasma Sources Sci. Technol. 31(5) (2022).
[24] E. Cleiren, S. Heijkers, M. Ramakers, A. Bogaerts, Dry Reforming of Methane in a Gliding Arc Plasmatron: Towards a Better Understanding of the Plasma Chemistry, ChemSusChem 10(20) (2017) 4025-4036.
[25] D. Khoe Dinh, D.H. Lee, Y.-H. Song, S. Jo, K.-T. Kim, Arc length control for efficiency enhancement of energy usage in plasma dry reforming process, J Co2 Util 28 (2018) 274-282.
[26] B. Wanten, S. Maerivoet, C. Vantomme, J. Slaets, G. Trenchev, A. Bogaerts, Dry reforming of methane in an atmospheric pressure glow discharge: Confining the plasma to expand the performance, J Co2 Util 56 (2022).
[27] M.K. Nikoo, N.A.S. Amin, Thermodynamic analysis of carbon dioxide reforming of methane in view of solid carbon formation, Fuel Process. Technol. 92(3) (2011) 678-691.
[28] X. Tu, J.C. Whitehead, Plasma-catalytic dry reforming of methane in an atmospheric dielectric barrier discharge: Understanding the synergistic effect at low temperature, Applied Catalysis B: Environmental 125 (2012) 439-448.
[29] J.-L. Liu, H.-W. Park, W.-J. Chung, W.-S. Ahn, D.-W. Park, Simulated biogas oxidative reforming in AC-pulsed gliding arc discharge, Chem. Eng. J. 285 (2016) 243-251.
[30] J.-B. Liu, X.-S. Li, J.-L. Liu, A.-M. Zhu, Insight into gliding arc (GA) plasma reduction of CO2 with H2: GA characteristics and reaction mechanism, Journal of Physics D: Applied Physics 52(28) (2019) 284001.
[31] A. Berthelot, A. Bogaerts, Modeling of CO2 Splitting in a Microwave Plasma: How to Improve the Conversion and Energy Efficiency, J. Phys. Chem. C 121(15) (2017) 8236-8251.
[32] W. Bongers, H. Bouwmeester, B. Wolf, F. Peeters, S. Welzel, D. van den Bekerom, N. den Harder, A. Goede, M. Graswinckel, P.W. Groen, J. Kopecki, M. Leins, G. van Rooij, A. Schulz, M. Walker, R. van de Sanden, Plasma-driven dissociation of CO2 for fuel synthesis, Plasma Process. Polym. 14(6) (2017) 1600126.
[33] J. Li, X.Q. Zhang, J. Shen, T.C. Ran, P. Chen, Y.X. Yin, Dissociation of CO2 by thermal plasma with contracting nozzle quenching, J Co2 Util 21 (2017) 72-76.
[34] I. Belov, V. Vermeiren, S. Paulussen, A. Bogaerts, Carbon dioxide dissociation in a microwave plasma reactor operating in a wide pressure range and different gas inlet configurations, J Co2 Util 24 (2018) 386-397.
[35] V. Vermeiren, A. Bogaerts, Plasma-Based CO2 Conversion: To Quench or Not to Quench?, J. Phys. Chem. C 124(34) (2020) 18401-18415.
[36] H. Zhang, Q.H. Tan, Q.X. Huang, K.Y. Wang, X. Tu, X.T. Zhao, C.F. Wu, J.H. Yan, X.D. Li, Boosting the Conversion of CO2 with Biochar to Clean CO in an Atmospheric Plasmatron: A Synergy of Plasma Chemistry and Thermochemistry, Acs Sustain Chem Eng 10(23) (2022) 7712-7725.
[37] H. Kim, S. Song, C.P. Tom, F. Xie, Carbon dioxide conversion in an atmospheric pressure microwave plasma reactor: Improving efficiencies by enhancing afterglow quenching, J Co2 Util 37 (2020) 240-247.
[38] D.H. Lee, K.-T. Kim, M.S. Cha, Y.-H. Song, Effect of excess oxygen in plasma reforming of diesel fuel, Int. J. Hydrog. Energy 35(10) (2010) 4668-4675.
[39] D.H. Lee, K.-T. Kim, H.S. Kang, S. Jo, Y.-H. Song, Optimization of NH3 Decomposition by Control of Discharge Mode in a Rotating Arc, Plasma Chem. Plasma Process. 34(1) (2014) 111-124.
[40] H. Zhang, W. Wang, X. Li, L. Han, M. Yan, Y. Zhong, X. Tu, Plasma activation of methane for hydrogen production in a N2 rotating gliding arc warm plasma: A chemical kinetics study, Chem. Eng. J. 345 (2018) 67-78.

[41] J. Martin-del-Campo, M. Uceda, S. Coulombe, J. Kopyscinski, Plasma-catalytic dry reforming of methane over Ni-supported catalysts in a rotating gliding arc ? Spouted bed reactor, J Co2 Util 46 (2021).
[42] S. Van Alphen, F. Jardali, J. Creel, G. Trenchev, R. Snyders, A. Bogaerts, Sustainable gas conversion by gliding arc plasmas: a new modelling approach for reactor design improvement, Sustain Energ Fuels 5(6) (2021) 1786-1800.
[43] W.M. Rohsenow, J.P. Hartnett, Y.I. Cho, Handbook of heat transfer, 3rd ed., McGraw-Hill, New York, 1998.
[44] N. Pinhao, A. Moura, J.B. Branco, J. Neves, Influence of gas expansion on process parameters in non-thermal plasma plug-flow reactors: A study applied to dry reforming of methane, Int. J. Hydrog. Energy 41(22) (2016) 9245-9255.
[45] D.K. Dinh, D.H. Lee, Y.-H. Song, S. Jo, K.-T. Kim, M. Iqbal, H. Kang, Efficient methane-to-acetylene conversion using low-current arcs, Rsc Adv 9(56) (2019) 32403-32413.
[46] H. Kang, S. Choi, C.M. Jung, K.-T. Kim, Y.-H. Song, D.H. Lee, Variations of methane conversion process with the geometrical effect in rotating gliding arc reactor, Int. J. Hydrog. Energy 45(55) (2020) 30009-30016.